Type of the article: Original article

Title: **Toward Truly Optimal IMRT Dose Distribution: Inverse Planning with Voxel-Specific Penalty**

Authors: Pavel Lougovski[(1)], Jordan LeNoach[(1)], Lei Zhu[(1)], Yunzhi Ma[(1)], Yair Censor[(2)], and Lei Xing[(1,*)]

[1)]Department of Radiation Oncology, Stanford University School of Medicine,
875 Blake Wilbur Drive, Stanford, CA 94305-5847, USA
[2)]Department of Mathematics, University of Haifa,
Mount Carmel, Haifa 31905, Israel

Short Title: Voxel-Specific Penalty for IMRT Dose Optimization

Keywords**:** IMRT, adaptive radiation therapy, dose optimization, inverse planning.

Abbreviations**:** IMRT – intensity-modulated radiation therapy

PTV – planning target volume

DVH – dose-volume histogram

OAR – organs at risk

[*)] Author to whom correspondence should be addressed.
Stanford University School of Medicine
Department of Radiation Oncology
875 Blake Wilbur Drive
Stanford, CA 94305-5847

E-mail: lei@stanford.edu
Phone: (650) 498 7896
Fax: (650) 498 4015

ABSTRACT

Purpose: To establish an inverse planning framework with adjustable voxel penalty for more conformal IMRT dose distribution as well as improved interactive controllability over the regional dose distribution of the resultant plan.

Materials and Method: In the proposed coarse-to-fine planning scheme, a conventional inverse planning with organ specific parameters is first performed. The voxel penalty scheme is then "switched on" by allowing the prescription dose to change on an individual voxel scale according to the deviation of the actual voxel dose from the ideally desired dose. The rationale here is intuitive: when the dose at a voxel does not meet its ideal dose, it simply implies that this voxel is not competitive enough when compared with the ones that have met their planning goal. In this case, increasing the penalty of the voxel by varying the prescription can boost its competitiveness and thus improve its dose. After the prescription adjustment, the plan is re-optimized. The dose adjustment/re-optimization procedure is repeated until the resultant dose distribution cannot be improved anymore. The prescription adjustment on a finer scale can be accomplished either automatically or manually. In the latter case, the regions/voxels where a dose improvement is needed are selected visually, unlike in the automatic case where the selection is done purely based on the difference of the actual dose at a given voxel and its ideal prescription. The performance of the proposed method is evaluated using a head and neck and a prostate case.

Results: An inverse planning framework with the voxel-specific penalty is established. By adjusting voxel prescriptions iteratively to boost the region where large mismatch between the actual calculated and desired doses occurs, substantial improvements can be achieved in the

final dose distribution. The proposed method is applied to a head and neck case and a prostate case. For the former case, a significant reduction in the maximum dose to the brainstem is achieved while the PTV dose coverage is greatly improved. The doses to other organs at risk are also reduced, ranging from 10% to 30%. For the prostate case, the use of the voxel penalty scheme also results in vast improvements to the final dose distribution. The PTV experiences improved dose uniformity and the mean dose to the rectum and bladder is reduced by as much as 15%.

Conclusion: Introduction of the spatially non-uniform and adjustable prescription provides room for further improvements of currently achievable dose distributions and equips the planner with an effective tool to modify IMRT dose distributions interactively. The technique is easily implementable in any existing inverse planning platform, which should facilitate clinical IMRT planning process and, in future, off-line/on-line adaptive IMRT.

INTRODUCTION

IMRT inverse planning has been envisaged as an automated process and its solution has been portrayed as optimal since the early days of its development (1-14). In reality, the output of a plan optimizer often does not satisfy clinical requirements and numerous trials are needed to finalize an IMRT treatment plan. Furthermore, an irksome aspect of the trial-and-error process is that there is little steering tool permitting the planner to shape the resultant dose distribution toward a solution that meets physician's requirements. On a more fundamental level, the success of optimization reported in the literature is often mathematical in nature because of the limited solution space predetermined by the objective function (15,16). The underlying deficiency, which is largely responsible for the above mentioned problem, is that all currently available IMRT planning systems are very much organ based in the sense that all optimization related parameters, such as the dose prescription and weighting factors, are specified on an organ level. While it is crucial to control the resultant dose on a regional or even an individual voxel level, the use of organ specific parameters makes it difficult and often impossible to balance the inter-voxel tradeoff because, fundamentally, one cannot control the response of a system to a level smaller than the scale of the system parameters. A possible solution is to extend the scale of the parameters to a voxel level. However, the practicality of specifying an enormous number of empirical parameters in clinical settings and the dramatically increased computational burden associated with that are the immediate concerns when a voxel-based penalty scheme is introduced.

Toward establishing a truly optimal inverse planning framework, we develop a coarse-to-fine voxel-based penalty scheme for IMRT dose optimization. Our goal here is quite modest. Instead of developing a full-fledged formalism with built-in voxel-based system parameters, we split the problem into two parts: (a) optimization with organ

specific parameters (i.e. conventional inverse planning) and (b) re-optimization with a voxel-specific prescription. The conventional planning provides us with a plan fairly close to our clinical goal, and usefully, with the knowledge on where and what kind of dosimetric improvements are needed (e.g., where the "hot/cold" spots are). The voxel-based scheme is only activated to tweak the final dose on a finer scale. This is what distinguishes our method from other schemes (15,19,28) where a voxel-based penalty is "switched on" all the time. The coarse-to-fine planning approach makes it possible for us to take the advantage of the useful features of both schemes, and to find a clinically more meaningful solution. In this work, the voxel-based penalty is realized by allowing the prescription to vary from the ideal value on a voxel-specific level. Both automated and interactive/manual dose fine-tuning schemes are implemented to facilitate clinical IMRT planning.

METHODS AND MATERIALS

1. Conventional inverse planning

A conventional IMRT inverse planning is first utilized to find a solution that meets our clinical goal in the domain of organ specific system parameters. Mathematically, the problem can be cast in terms of a quadratic objective function that is minimized to find optimal beamlet intensity:

$$\textit{minimize} \qquad F(x) = \sum_{\sigma=1}^{S} \lambda_\sigma \left\| D^\sigma - d^\sigma \right\| \qquad [1]$$

$$\textit{s.t.} \qquad D^\sigma = A_\sigma x, \qquad \sigma = 1, \cdots, S; \quad x \geq 0.$$

Here σ is the index of a structure (*i.e.*, an organ at risk (OAR) or a target) involved in the planning, λ_σ is a structure-specific weighting factor, D^σ and d^σ are the calculated and prescribed doses, respectively, and x is the vector of beamlet intensities. We set the initial

values of the prescription d^{σ} to 0 for all OARs, and to 1 for all targets, and refer to this prescription as the ideal prescription throughout the paper. The zero choice of the ideal dose prescription to the OARs is practically motivated by the desire to have the algorithm to continuously drive the doses to the OARs down when there is room for such an improvement. The calculated dose D^{σ} and the beamlet intensity x are related by the beamlet kernel matrix A_{σ}. The optimization of Eq. [1] is implemented on the MATLAB platform by using the MOSEK optimization package (17,18). The output of the optimization calculation is the vector of beamlet intensities (or fluence map of all incident beams) for any given set of prescription d^{σ} and weight λ_{σ}. The initial values of the weight factors λ_{σ} can be arbitrary. Our algorithm will automatically compensate for less optimal values of λ_{σ} through the fine-tuning of the voxel prescription. It is, however, practically useful to set λ_{σ} to a value as close to the optimal as possible. In this way, the effect of fine-tuning of voxel prescription will be more pronounced.

2. Adjustment of the voxel prescription

Our planning approach can be outlined as an iterative process with two basic operations: (a) dose optimization for a given prescription distribution; (b) updating of the voxel-specific prescription based on the comparison of the calculated and *ideal* doses at each voxel for the next cycle of optimization. The differential adjustment of voxel prescription is a simple way of tweaking the tradeoff between different voxels in the same or different structures. The iterative prescription adjustment can be implemented in a fully automated or manual (interactive) manner to meet different clinical needs. In the following we first outline the main idea of our prescription adjustment method, which is used in the subsequent implementations of automated or manual voxel penalty tuning method.

A set of starting dose prescriptions, say, the ideal dose distribution for the patient, $\{d_I{}^\sigma\}$, is first assigned to the structures and the system defined by Eq. [1] is solved for $d^\sigma = d_I{}^\sigma$. This step is essentially the conventional inverse planning. We then adjust the prescription for individual voxels based on the deviation of the calculated dose from the ideal dose at the corresponding voxel. Mathematically, the adjusted prescription reads,

$$d_2{}^\sigma = d_1{}^\sigma + \Delta d_1{}^\sigma = d_1{}^\sigma + \gamma(d_I{}^\sigma - D_1^\sigma), \qquad [2]$$

here $d_1{}^\sigma$ is the prescription used to solve Eq. [1] with D_1^σ being the solution. A user-defined constant γ determines the proportion of the dosimetric mismatch used to correct the prescription. In this work γ is set to 1 empirically; other values of γ are acceptable, but they may change the convergence behavior of the algorithm. Repeating the above adjustment procedure K times results in the voxel-specific prescription d_{K+1}^σ:

$$d_{K+1}^\sigma = d_K^\sigma + \Delta d_K^\sigma = d_K^\sigma + \gamma(d_I^\sigma - D_K^\sigma), \quad \sigma = 1, \cdots, S. \qquad [3]$$

2.1. Automated adjustment of voxel prescription

In this scheme, the above optimization and prescription adjustment are repeated automatically until the dose distribution cannot be improved any further or when a predefined stopping criterion is met. Practically, we choose to stop when the difference between two consecutive prescription adjustments becomes less than a pre-specified constant. That is, $\Delta d_K^\sigma - \Delta d_{K+1}^\sigma \le C$, where C is a constant.

2.2. Manual prescription adjustment

A major deficiency that hinders the current clinical IMRT planning workflow is the lack of direct control over the detailed 3D dose distribution. Thus, a considerable effort is often

required to obtain a clinically acceptable plan. A voxel-specific penalty provides an interactive inverse planning scheme and offers the planner an effective mechanism to fine-tune an IMRT dose distribution towards a desirable direction of improvement. In practice, after an IMRT plan is computed, the dose in one or more sub-volumes of a structure may need to be changed locally. The key to the enhancement of the degree of control over the regional dose is to establish an effective link between the local dose and the system variables through a voxel penalty modulation. Our optimization scheme does that through a modified quadratic objective function; the voxel-dependent prescription "modulates" the inter-voxel tradeoff. But other ways of changing the voxel penalty can also be implemented (19-22). In our approach, the voxel doses that need to be modified are identified visually either on the isodose layouts or DVH curves. The local prescriptions of the relevant voxels are then increased/decreased, in order to drive the regional doses towards desired values. Upon re-optimizing the plan with adjusted prescription, the doses at the identified areas (or DVH segments) are usually improved. The planner analyses the new dose distribution and decides whether a further adjustment is necessary. The procedure can be repeated until the dose to a region (organ) cannot be further improved without severely deteriorating the dose to other regions (organs). This provides an iterative IMRT dose fine-tuning environment.

3. Case study

Two clinical cases – a head and neck and a prostate case – were used to test the method in both automated and manual regimes. The running time for each optimization step was about 1 minute on a desktop computer with Intel Core 2 Duo 2.66 GHz CPU and 3.25 GB of RAM. The total planning time did not exceed 10 minutes for the cases studied. It can be further decreased by using commercial treatment planning algorithms. The results were compared with the corresponding IMRT plans obtained using a conventional method.

In the head and neck case, a beam configuration with seven treatment fields at 20, 120, 145, 180, 215, 240 and 340 degrees was chosen, each field containing an array of 16-by-20 beamlets. The sensitive structures included the brainstem, optic chiasm/nerves, optic lens, left parotid, larynx and spinal cord. They were prescribed the ideal dose of zero. The ideal dose for the PTV was set to 66 Gy. No attempt to spare the right parotid was made because it overlaps with the PTV.

For the prostate case, a setup with five treatment fields at 35, 110, 180, 250 and 325 degrees was used. The rectum, bladder, penile bulb, and seminal vesicles (SV) were included as the sensitive structures. The ideal dose d_I^{σ} for them was set to zero. The inclusion of the SV into inverse planning depends on the staging of the patient. For instance, in case of the early stage prostate cancer the SV is not a part of the planning. The PTV was assigned a uniform ideal dose of 74 Gy in the conventional inverse planning calculation.

RESULTS

1. Head and neck case

1.1 Automated prescription adjustment

We first produced a conventional IMRT plan with the ideal prescription of 66 Gy to the PTV and 0 Gy to the sensitive structures. The corresponding DVHs are shown in Fig. 1 (solid lines). To reduce the dose to the cord, brainstem and left parotid while improving the PTV dose coverage, the automated prescription adjustment and re-optimization were carried out for the case, using the method described in the Methods and Material section (subsection 2.1). The prescription adjustment was simultaneously applied to the PTV and the sensitive structures. The optimal plan was achieved after five cycles of re-optimizations and the results are depicted in Fig. 1 (dashed lines). A further comparison of the conventional IMRT

and the automatically updated non-uniform prescription plans is illustrated in Fig. 2 using the isodose plots. Here, the contour lines at 95%, 65%, and 30% of the PTV ideal dose (66 Gy) are shown. The dose distributions confirm that there is a great reduction of irradiation to the tissue surrounding the PTV in addition to the reduction of hot spots in the PTV in the plan obtained using the proposed method. The dosimetric statistics of the conventional and prescription adjusted plans is summarized in Table I. It is evident that the maximum dose to the brainstem and the cord is reduced by as much as 20% when compared to the conventional IMRT plan, without compromising the dose to other organs and the PTV.

1.2. Manual prescription adjustment

The starting point for the proposed interactive planning scheme, likewise in the automated case, is a conventional IMRT plan with the structure specific ideal prescription. After the conventional planning was performed, the resulting isodose plot (Fig. 3a) was examined visually. In this particular axial slice, a significant part of the brainstem receives a dose over 22Gy. We also notice a hot spot in the PTV in the close proximity of the brainstem. Suppose that the clinical objectives are to improve the dose to the brainstem and to suppress or at least move away the hot spot. For that, we first graphically locate the brainstem voxels receiving the dose of 22Gy or higher. The prescription adjustment is then computed using Eq. [2] and re-optimization of the dose is performed with the adjusted brainstem prescription (Fig. 3b). The new dose distribution in Fig. 3b shows that the dose reduction in brainstem is achieved with a single prescription modification and re-optimization. The dose distribution in other structures remains essentially unchanged, illustrating the utility of the proposed method. In order to accomplish our second objective – to suppress the hot spot in the PTV – we adjust the prescription for the PTV voxels using Eq. [3]. The resultant dose distribution is displayed in Fig. 3c. One can clearly see that the re-optimized plan with the adjusted prescription significantly reduced the hot spot and

pulled it away from the sensitive structures. While it may happen that the improvement in the dose to a structure may be accompanied by adverse dosimetric effect(s) at other points in the same or different structures, from a clinical point of view, we emphasize that some dose distributions are more acceptable than others, even if they may have similar DVHs. Being able to maneuver the dose distribution to meet a specific clinical need efficiently is a highly desirable feature in clinical practice.

2. Prostate case

Figure 4 and Table II represent the results of a side-by-side comparison of two treatment plans obtained using the conventional and proposed automatic voxel prescription adjustment techniques. Five cycles of re-optimization with voxel prescription adjustment to all involved structures were performed to obtain the presented results. The corresponding DVHs are plotted in Fig.4 (dashed lines). Similarly to the previous case study, we observe a substantial reduction in the dose to the rectum and bladder when compared to the conventional IMRT plan. At the same time the PTV dose conformity and uniformity are improved by adaptively adjusting the voxel prescription. According to the statistics summarized in Table II, the mean dose reduction for the bladder and rectum is as large as 20%. It is useful to note that the improvement is achieved by the enabled inter-voxel dosimetric tradeoff, not at the cost of the dose deterioration in other structures or higher PTV dose inhomogeneity.

DISCUSSION

Dose optimization is a process of finding a fine balance between various competing objectives (23). In conventional optimization with uniform (or a fixed non-uniform) dose prescription, the accessible solution space is populated by the plans that minimize the objective function Eq. [1] with structure specific parameters. Adding mean (max) dose or dose –volume constraints to conventional planning can certainly improve plan's quality.

However, it does not change the space of optimal solution. One simply selects a different solution according to the added constraints. On contrary, by "switching on" the voxel penalty, inter-voxel tradeoff that is "fixed" in conventional inverse planning becomes tunable, leading to an enlarged solution space and allowing us to find solutions that otherwise would not be possible. In our implementation, the voxel prescription is now a part of the optimization parameters and is optimized by using a coarse-to-fine strategy. In the language of multi-objective optimization (24-26), with the introduction of voxel-based penalty scheme, the solutions corresponding to different prescription distributions (or different inter-voxel tradeoffs) contribute to a new Pareto front. The conventional IMRT solutions represent just a subset of the enlarged solution space. In reality, there is no easy way to know which specific form of the non-uniform dose prescription can lead to a clinically optimal solution and the proposed coarse-to-fine algorithm provides a method to navigate through the enlarged solution space and find the truly optimal plan.

It is important to realize that the inherent capabilities of the voxels in achieving their dosimetric goals are generally not equivalent and this causes inter-voxel competition even within the same structure (27,28). Depending on the patient's geometry, beam modality and field configuration, some regions may have a better chance to meet their ideal prescription than others, and *vice versa*. The final dose at a voxel depends on both the prescription and the dosimetric capability of the voxel. In the proposed inverse planning formalism, the inter-voxel tradeoff is effectively modified by varying the voxel prescription, leading to a significant dosimetric improvement as compared to that of the conventional inverse planning scheme. To illustrate the role of the voxel penalty, in Fig. 5 we plot the mismatch between the ideal prescription and the actual dose for a few selected voxels as a function of the dose re-optimization step. The positive (negative) value of the mismatch indicates that the voxel is under-dosed (overdosed) with respect to its ideal

prescription. For the target voxel #1 and the cord voxel #1, the doses after conventional planning are quite far from their ideal dose values. These are the voxels that are not inherently competitive and an adjustment of their prescriptions effectively boosts their capabilities in achieving their dosimetric goals. On the other hand, for the target voxel #2 and the cord voxel #2 the prescriptions remain almost unchanged during the re-optimization process, primarily because the doses at these voxels are already very close to the ideal values. By adjusting the inter-voxel tradeoff, the doses at those less competitive voxels are improved without or with little dosimetric sacrifices at other voxels.

Convergence behavior is an important feature of any iteration-based planning algorithm. We found that, for the head and neck and the prostate cases studied here, the convergence is readily achieved after 3~5 successive prescription adjustments. In Fig. 6 we plot the value of the objective function for the spinal cord as a function of the number of prescription adjustments. One can see that it converges after three iterations. Similar behavior has been observed for other sensitive structures and the PTVs. Since the convergence occurs rapidly, the computational time does not constitute a major obstacle for the implementation of the proposed method. The size of the problem and the constraints used remain the major factors that influence the computational speed. In fact, the proposed approach has the potential of significantly reducing the time and effort of IMRT planning because of the reduced need for trial-and-errors that is necessary in conventional inverse planning.

Depending on the resultant dose distribution after the initial IMRT planning, and the clinical objective, the iterative prescription adjustment scheme can be performed on either all voxels or only the voxels in one or several selected structures. In addition, the adjustment of the local prescription can be performed sequentially or simultaneously. To illustrate this, we compare in Fig. 7 the DVHs of the conventional head and neck plan and

the plan with prescription modulation limited to the PTV. One can see that for the later plan the PTV dose distribution (dashed curve in Fig. 7) becomes more uniform even when compared to the solution with prescription modulations imposed on all structures (dashed curves in Fig. 1). Because of the improvement of overdosing in the PTV, the doses to the brainstem, cord and parotids are also, remarkably, reduced (dashed lines Fig. 7).

CONCLUSIONS

Conventional objective function with structure specific weighting and prescription is deficient in that it "freezes" the inter-voxel tradeoff. In reality, solutions attainable in the conventional approach represent a subset of the plans accessible in a more general voxel penalty framework. IMRT dose optimization can be improved significantly in both the plan quality and the maneuverability of the planning process by allowing inter-voxel tradeoffs. Generally, there are two possible ways to include voxel penalty: (1) Introduce a voxel-based penalty function from the beginning and optimizing the system in a brute-force fashion; and (2) Switch on the voxel penalty after the conventional planning is done and then iteratively modify the voxel penalty towards a more clinically meaningful solution. In this work, the latter approach has been investigated as it is more intuitive and computationally manageable. It has been shown that the use of the voxel penalty scheme permits us to find solutions from a much larger solution space, that otherwise would be inaccessible. The presented automated voxel-based iterative prescription adjustment approach produces significantly improved treatment plans. When the voxel penalty is tuned manually, the proposed technique provides effective means for modifying the local doses and makes interactive IMRT planning (or interactive dose or DVH shaping) straightforward. This is not only significant for current IMRT and modulated arc (tomotherapy and volumetric arc therapy) practice, but even more valuable for the future on-line/off-line adaptive radiation therapy re-planning and/or biologically-conformal radiation therapy planning to "paint" and "sculpt" dose distributions in accordance with biological imaging information.

The proposed method is not restricted to a quadratic objective function – it is applicable to any other forms of objective function. The intra-voxel tradeoff is a general issue in IMRT and VMAT inverse planning, and the methodologies and findings presented in the paper will have broader implications and are also useful for future investigations using biological models.

Conflict of Interest Statement: There is no conflict of interest.

ACKNOWLEDGEMENTS

We wish to thank Drs. Yong Yang, Christian Cotrutz, and Quynh Le for useful discussions. This project was supported by National Cancer Institute (1R01 CA104205) and a summer student fellowship from the Department of Physics of Stanford University. The work of Y.C. was partially supported by Award Number R01HL070472 from the National Heart, Lung, and Blood Institute.

280 **FIGURES AND TABLES**

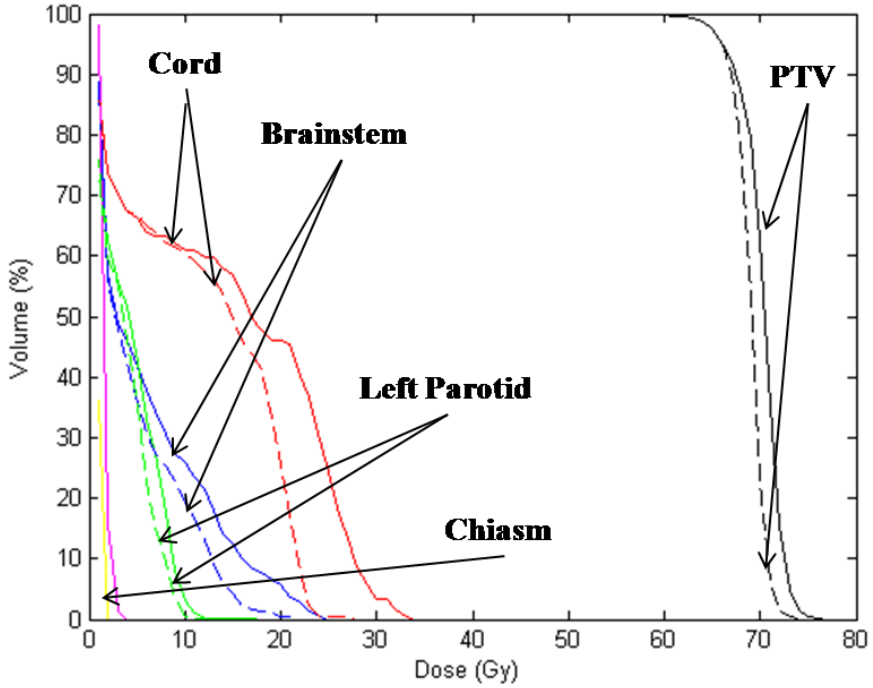

Figure 1 DVHs of the head and neck IMRT plans obtained using the conventional approach with the fixed prescription (solid curves) and the proposed strategy of automated voxel prescription adjustment (dashed curves).

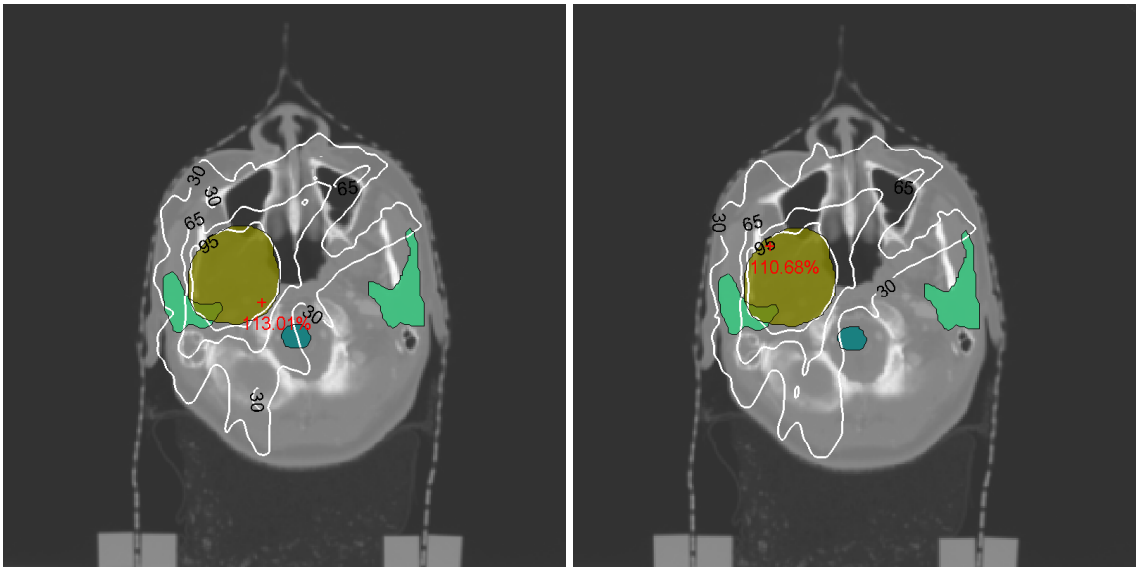

Figure 2 Head and neck plan dose distributions before (left) and after voxel prescription adjustment (right). The PTV and the sensitive structures (brainstem, left and right parotids) are shown in

different colors. The isodose lines correspond to 95%, 65% and 30% of the prescribed dose (66 Gy). Hotspots are marked with red crosses.

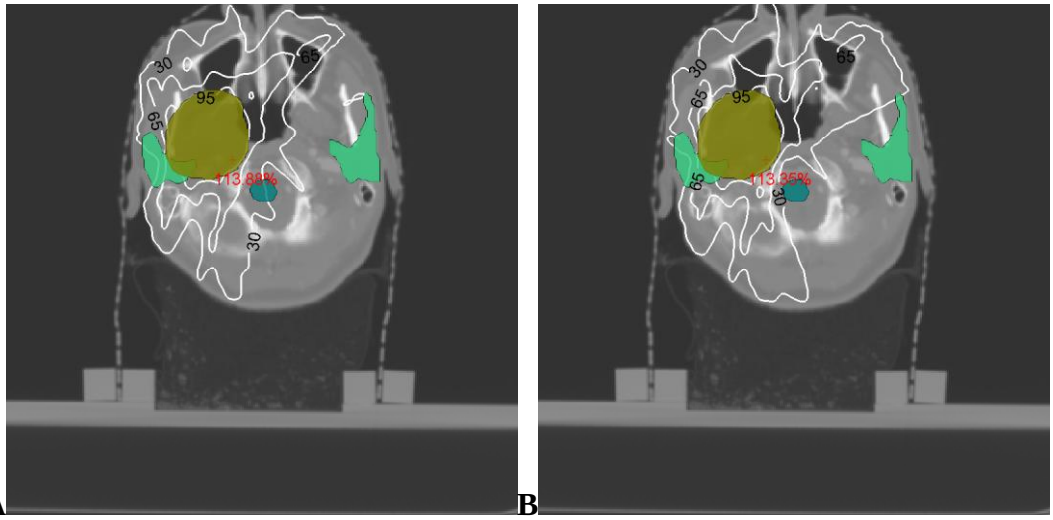

A **B**

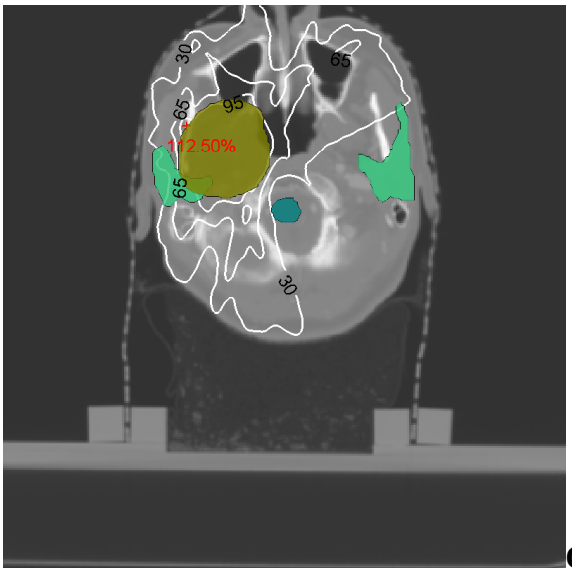

C

Figure 3 Head and neck plan dose distributions for the manual voxel prescription adjustment method. A (top left): before the prescription adjustment. B (top right): after the adjustment of the brainstem prescription. C (bottom center): after the adjustment of the brainstem and PTV prescriptions. The PTV and the sensitive structures (brainstem, left and right parotids) are shown in different colors. The iso-dose lines correspond to 95%, 65% and 30% of the prescribed dose (66 Gy). Hotspots are marked with red crosses.

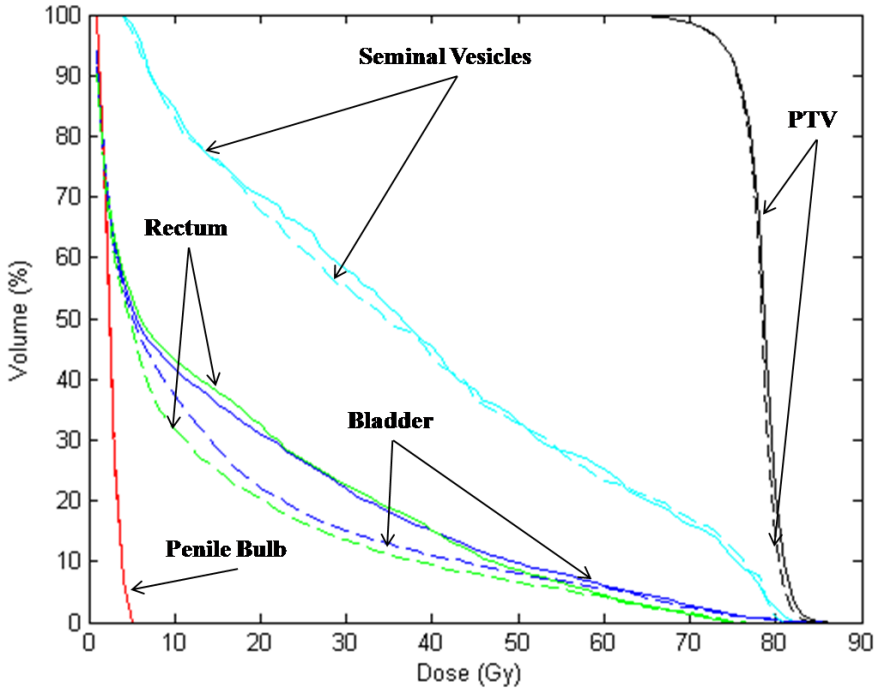

Figure 4 DVHs of the prostate IMRT plans obtained using the conventional approach with the fixed prescription (solid curves) and the proposed strategy of automated voxel prescription adjustment (dashed curves).

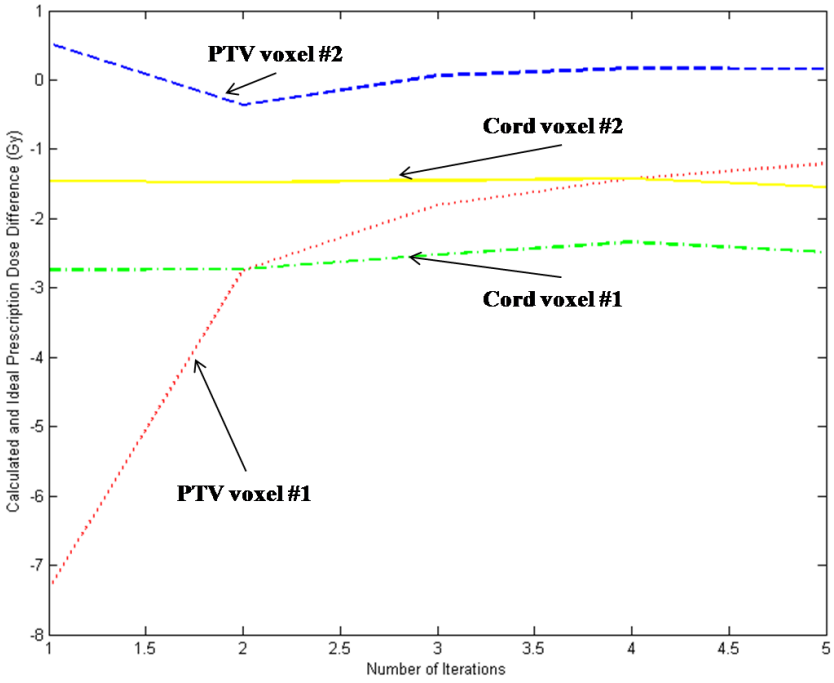

Figure 5 The difference between the ideal prescription and the calculated dose for selected voxels in the PTV and the cord for the head and neck case as a function of iteration number.

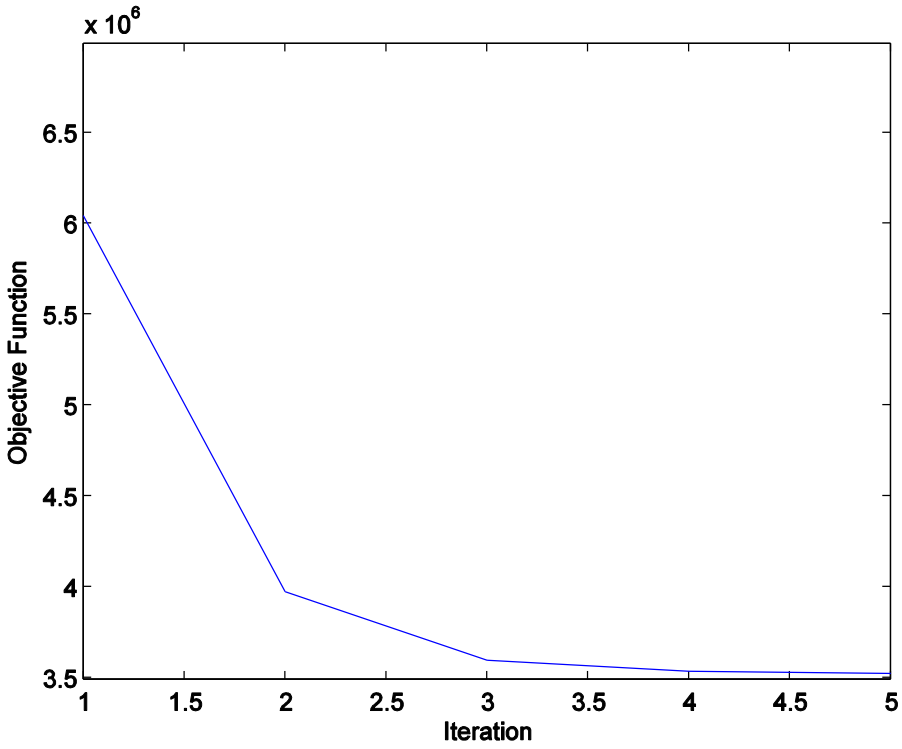

Figure 6 The value of the spinal cord objective as a function of iteration number.

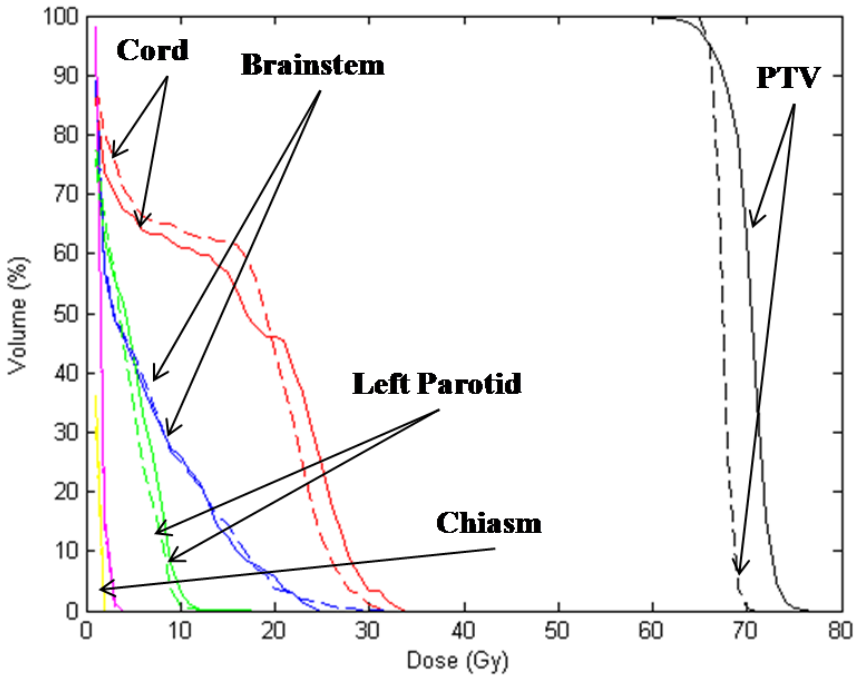

Figure 7 The automated prescription adjustment method applied only to the PTV for the head and neck case. Solid lines represent the DVHs for the conventional IMRT plan with the fixed ideal prescription. Dashed lines correspond to the plan obtained with automated prescription adjustment.

Regions	Conventional	Adjusted
PTV	% vol > 66Gy = 95% maximum = 76.04Gy minimum = 58.02Gy mean = 70.18	% vol > 66Gy = 95% maximum = 74.62Gy minimum = 58.57Gy mean = 68.93
Brainstem	maximum = 24.63Gy mean = 6.22Gy	maximum = 20.73Gy mean = 4.99Gy
Larynx	maximum = 3.18Gy	maximum = 3.17Gy

	mean = 1.58Gy	mean = 1.58Gy
Chiasm	maximum = 1.13Gy mean = 0.93Gy	maximum = 1.14Gy mean = 0.92Gy
Cord	maximum = 33.6Gy mean = 14.98Gy	maximum = 26.55Gy mean = 12.29Gy
Left Parotid	maximum = 17.06Gy	maximum = 15.74Gy
	mean = 4.33Gy	mean = 3.43Gy

Table I Dosimetric statistics of the head and neck case before and after prescription adjustment. Corresponding DVHs and dose distributions are shown on Figs. 1 and 2.

Regions	Conventional	Adjusted
PTV	% vol > 74Gy = 95% maximum = 86.32Gy minimum = 62.73Gy mean = 78.42	% vol > 74Gy = 95% maximum = 84.77Gy minimum = 63.45Gy mean = 78.06
Rectum	maximum = 74.00Gy mean = 16.47Gy	maximum = 76.85Gy mean = 12.36Gy
Bladder	maximum = 85.47Gy	maximum = 83.64Gy
	mean = 16.61Gy	mean = 13.91Gy
Seminal Vesicles	maximum = 82.47Gy mean = 38.55Gy	maximum = 80.47Gy mean = 37.86Gy

Penile Bulb	maximum = 4.83Gy mean = 2.53Gy	maximum = 4.80Gy mean = 2.56Gy

Table II Dosimetric statistics of the head and neck case before and after prescription adjustment. Corresponding DVHs are shown in Fig. 4.

REFERENCES

1 Brahme, A., Roos, J. E. & Lax, I. Solution of an integral equation encountered in rotation therapy. *Phys. Med. Biol. 27*, 1221-1229 (1982).

2 Censor, Y., Altschuler, M. D. & Powlis, W. D. A computational solution of the inverse problem in radiation-therapy treatment planning. *Appl. Math. Comput. 25*, 57-87 (1988).

3 Censor, Y., Altschuler, M. D. & Powlis, W. D. On the use of Cimmino's simultaneous projections method for computing a solution of the inverse problem in radiation therapy treatment planning. *Inverse Probl. 4*, 607-623 (1988).

4 Bortfeld, T., Burkelbach, J., Boesecke, R. & Schlegel, W. Methods of image reconstruction from projections applied to conformation radiotherapy. *Phys. Med. Biol. 35*, 1423-1434 (1990).

5 Xing, L., Wu, Q., Yang, Y. & Boyer, A. in *Intensity-Modulated Radiation Therapy: A Clinical Perspective* eds AJ Mundt & JC Roeske) 20-52 (BC Decker Inc, 2005).

6 Bogner, L., Scherer, J., Treutwein, M., Hartmann, M., Gum, F. & Amediek, A. Verification of IMRT: Techniques and problems. *Strahlenther. Onkol. 180*, 340-350 (2004).

7 Yang, Y. & Xing, L. Clinical knowledge-based inverse treatment planning. *Phys Med Biol 49*, 5101-5117 (2004).

8 Wu, Q. & Mohan, R. Algorithms and functionality of an intensity modulated radiotherapy optimization system. *Medical Physics 27*, 701-711 (2000).

9 Deasy, J. O. Multiple local minima in radiotherapy optimization problems with dose-volume constraints. *Medical Physics 24*, 1157-1161 (1997).

10 Webb, S. Optimization by simulated annealing of three-dimensional conformal treatment planning for radiation fields defined by a multileaf collimator. *Physics in Medicine & Biology 36*, 1201-1226 (1991).

11 Lee, E. K., Fox, T. & Crocker, I. Simultaneous beam geometry and intensity map optimization in intensity-modulated radiation therapy. *Int J Radiat Oncol Biol Phys 64*, 301-320 (2006).

12 Ziegenhein, P., Wilkens, J. J., Nill, S., Ludwig, T. & Oelfke, U. Speed optimized influence matrix processing in inverse treatment planning tools. *Physics in medicine and biology 53*, N157-164 (2008).

13 Bogner, L., Hartmann, M., Rickhey, M. & Moravek, Z. Application of an inverse kernel concept to Monte Carlo based IMRT. *Med. Phys. 33*, 4749-4757 (2006).

14 Zhang, P. P., Wu, J., Dean, D., Xing, L., Xue, J. Y., Maciunas, R. & Sibata, C. Plug pattern optimization for gamma knife radiosurgery treatment planning. *International Journal of Radiation Oncology Biology Physics 55*, 420-427 (2003).

15 Cotrutz, C. & Xing, L. Using voxel-dependent importance factors for interactive DVH-based dose optimization. *Physics in Medicine & Biology 47*, 1659-1669 (2002).

16 Cotrutz, C. & Xing, L. IMRT dose shaping using regionally variable penalty scheme. *Medical Physics 30*, 544-551 (2003).

17 Zhu, L., Lee, L., Ma, Y., Ye, Y., Mazzeo, R. & Xing, L. Using total-variation regularization for intensity modulated radiation therapy inverse planning with field-specific numbers of segments. *Physics in medicine and biology 53*, 6653-6672 (2008).

18 Zhu, L. & Xing, L. Search for IMRT inverse plans with piecewise constant fluence maps using compressed sensing techniques. *Medical physics 36*, 1895-1905 (2009).

19 Zhang, X. D., Wang, X. C., Dong, L., Liu, H. & Mohan, R. A sensitivity-guided algorithm for automated determination of IMRT objective function parameters. *Med. Phys. 33*, 2935-2944 (2006).

20 Wilkens, J. J., Alaly, J. R., Zakarian, K., Thorstad, W. L. & Deasy, J. O. IMRT treatment planning based on prioritizing prescription goals. *Phys. Med. Biol. 52*, 1675-1692 (2007).

21 Yan, H., Yin, F. F., Guan, H. Q. & Kim, J. H. AI-guided parameter optimization in inverse treatment planning. *Phys. Med. Biol. 48*, 3565-3580 (2003).

22 Meyer, J., Phillips, M. H., Cho, P. S., Kalet, I. & Doctor, J. N. Application of influence diagrams to prostate intensity-modulated radiation therapy plan selection. *Phys. Med. Biol. 49*, 1637-1653 (2004).

23 Xing, L., Li, J. G., Donaldson, S., Le, Q. T. & Boyer, A. L. Optimization of importance factors in inverse planning. *Physics in Medicine & Biology 44*, 2525-2536 (1999).

24 Cotrutz, C., Lahanas, M., Kappas, C. & Baltas, D. A multiobjective gradient-based dose optimization algorithm for external beam conformal radiotherapy. *Physics in Medicine & Biology 46*, 2161-2175 (2001).

25 Schreibmann, E., Lahanas, M., Xing, L. & Baltas, D. Multiobjective evolutionary optimization of the number of beams, their orientations and weights for intensity-modulated radiation therapy. *Phys Med Biol 49*, 747-770 (2004).

26 Spalke, T., Craft, D. & Bortfeld, T. Analyzing the main trade-offs in multiobjective radiation therapy treatment planning databases. *Phys Med Biol 54*, 3741-3754 (2009).

27 Shou, Z., Yang, Y., Cotrutz, C., Levy, D. & Xing, L. Quantitation of the a priori dosimetric capabilities of spatial points in inverse planning and its significant implication in defining IMRT solution space. *Phys Med Biol 50*, 1469-1482 (2005).

28 Yang, Y. & Xing, L. Inverse treatment planning with adaptively evolving voxel-dependent penalty scheme. *Med Phys 31*, 2839-2844 (2004).

Figures and Tables Captions

Table I Dosimetric statistics of the head and neck case before and after prescription adjustment. Corresponding DVHs and dose distributions are shown on Figs. 1 and 2.

Table II Dosimetric statistics of the head and neck case before and after prescription adjustment. Corresponding DVHs are shown in Fig. 4.

Figure 1 DVHs of the head and neck IMRT plans obtained using the conventional approach with the fixed prescription (solid curves) and the proposed strategy of automated voxel prescription adjustment (dashed curves).

Figure 2 Head and neck plan dose distributions before (left) and after voxel prescription adjustment (right). The PTV and the sensitive structures (brainstem, left and right parotids) are shown in different colors. The isodose lines correspond to 95%, 65% and 30% of the prescribed dose (66 Gy). Hotspots are marked with red crosses.

Figure 3 Head and neck plan dose distributions for the manual voxel prescription adjustment method. A (top left): before the prescription adjustment. B (top right): after the adjustment of the brainstem prescription. C (bottom center): after the adjustment of the brainstem and PTV prescriptions. The PTV and the sensitive structures (brainstem, left and right parotids) are shown in different colors. The iso-dose lines correspond to 95%, 65% and 30% of the prescribed dose (66 Gy). Hotspots are marked with red crosses.

Figure 4 DVHs of the prostate IMRT plans obtained using the conventional approach with the fixed prescription (solid curves) and the proposed strategy of automated voxel prescription adjustment (dashed curves).

Figure 5 The difference between the ideal prescription and the calculated dose for selected voxels in the PTV and the cord for the head and neck case as a function of iteration number.

Figure 6 The value of the spinal cord objective as a function of iteration number.

Figure 7 The automated prescription adjustment method applied only to the PTV for the head and neck case. Solid lines represent the DVHs for the conventional IMRT plan with the fixed ideal prescription. Dashed lines correspond to the plan obtained with automated prescription adjustment.